Modulation of Nitrated Lipid Signaling by Multidrug Resistance Protein 1 (MRP1): Glutathione Conjugation and MRP1-Mediated Efflux Inhibit Nitrolinoleic Acid-Induced, PPARγ-Dependent Transcription Activation†

Richard L. Alexander,‡ Darcy J. P. Bates,‡ Marcus W. Wright,§ S. Bruce King,§ and Charles S. Morrow*,‡

Department of Biochemistry, Wake Forest University School of Medicine, Medical Center Boulevard, and Department of Chemistry, Wake Forest University, Winston-Salem, North Carolina 27157

Received March 21, 2006; Revised Manuscript Received April 27, 2006

ABSTRACT: Recent data has shown that nitrolinoleic acid (LNO_2), an electrophilic derivative of linoleic acid, has several important bioactivities including antiinflammatory, antiplatelet, vasorelaxation, and—as a novel potent ligand of PPARγ—transcription regulating activities. Moreover, LNO_2 is formed in abundance in vivo at levels sufficient to mediate these bioactivities. In order to investigate the role of glutathione conjugation and MRP1-mediated efflux in the regulation of PPARγ-dependent LNO_2 signaling, regioisomers of LNO_2 were synthesized and characterized. Analysis by 1D and 2D ^{1}H and ^{13}C NMR revealed that the LNO_2 preparation consisted of four, rather than two, nitrated regioisomers in approximately equal abundance. At physiologic pH and intracellular glutathione levels, LNO_2 was rapidly and quantitatively converted to glutathione conjugates (LNO_2−SG) via Michael addition. MRP1 mediated efficient ATP-dependent transport of LNO_2−SG. Using a PPRE-containing reporter gene transiently transfected into MRP-poor MCF7/WT cells, we verified that the LNO_2 mixture was a potent activator of PPARγ-dependent transcription. However, expression of MRP1 in the stably transduced MCF7 derivative, MCF7/MRP1-10, resulted in strong inhibition of LNO_2-induced transcription activation. Taken together, these results suggest that glutathione conjugation and MRP1-mediated conjugate transport can attenuate LNO_2 bioactivity and thereby play important roles in the regulation of cellular signaling by LNO_2.

The peroxisomal proliferator-activated receptor γ[1] (PPARγ) is an important nuclear receptor that regulates many cellular functions such as lipid homeostasis, adipocyte differentiation, and inflammatory signaling (*1*−*4*). Upon ligand binding, PPARγ facilitates heterodimerization with the retinoid X receptor (RXR), recruitment of transcriptional coeffectors, and binding of the complex to PPAR responsive elements to regulate gene expression (*5*−*7*). PPARγ is the target for the thiazolidinedione drugs used in the treatment of diabetes (*8*), and many studies have demonstrated PPARγ-dependent transactivation by lipid metabolites (*9*−*12*). However, the most important endogenous ligands for PPARγ are still unknown.

Recent evidence has suggested that the electrophilic, nitrated derivatives of linoleic acid, nitrolinoleic acid (LNO_2), are important lipid mediators of several biological processes such as antiinflammation (*13*), antiplatelet activity (*14*), and vasorelaxation (*15*, *16*). Furthermore, recent studies have shown that LNO_2 is a potent activator of PPARγ-dependent transcription indicating that LNO_2 and other nitrated lipids such as nitrooleic acid (OA-NO_2) could prove to be important endogenous ligands for PPARγ (*17*, *18*). Indeed, LNO_2 and OA-NO_2 are found in plasma and red blood cells at levels sufficient to mediate activation of PPARγ-dependent transcription (*16*, *17*, *19*).

We speculated that LNO_2—like 15-deoxy-$\Delta^{12,14}$prostaglandin J_2 (15-d-PGJ_2), another electrophilic lipid activator of PPARγ previously studied in our laboratory (*20*, *21*)—is likely to form intracellular conjugates with glutathione (GSH) that can be removed by the efflux transporter, MRP1. Moreover, we hypothesized that GSH conjugation and MRP1 transport may represent important processes in the regulation of cellular response to LNO_2. Thus, in the present studies we describe the synthesis, purification, and structural characterization LNO_2 and its glutathione conjugates. Using in vitro and cellular models derived from MRP-poor (MCF7/WT) and MRP1-expressing (MCF7/MRP1-10) MCF7 derivatives, we demonstrate that GSH conjugation of LNO_2 and MRP1-mediated efflux of this conjugate, LNO_2−SG, profoundly inhibits LNO_2-induced PPARγ-dependent transcription.

† This work was supported by NIH Grant CA 70338 (C.S.M.) and T32 ES007331 (R.L.A.).

* To whom all correspondence should be addressed at Department of Biochemistry, Wake Forest University School of Medicine, Medical Center Boulevard, Winston-Salem, NC 27157. Tel: (336) 713-7218. Fax: (336) 716−7671. E-mail: cmorrow@wfubmc.edu.

‡ Department of Biochemistry, Wake Forest University School of Medicine.

§ Department of Chemistry.

[1] Abbreviations: AMP-PCP, β,γ-methyleneadenosine 5′-triphosphate; ESI, electrospray ionization; GSH, glutathione; LNO_2, (9, 10, 12, or 13)-nitro-9-*cis*,12-*cis*-octadecadienoic acid (nitrolinoleic acid); LNO_2−SG, glutathione conjugates of LNO_2; MRP1, multidrug resistance (or resistance-associated) protein 1 (ABCC1); MS, mass spectrometry; OA-NO_2, (9 or 10)-nitro-9-*cis*-octadecenoic acid (nitrooleic acid); 15-d-PGJ_2 and 15-d-PGJ_2−SG, 15-deoxy-$\Delta^{12,14}$prostaglandin J_2 and its glutathione conjugate, respectively; PPAR, peroxisomal proliferator-activated receptor; PPRE, PPAR responsive element.

10.1021/bi0605639 CCC: $33.50
Published on Web 06/06/2006

EXPERIMENTAL PROCEDURES

Synthesis and NMR Analysis of LNO_2. The synthesis of LNO_2 was modified from a previously published source (*17*). Mercury(II) chloride (3.8 g, 14 mmol), phenylselenyl bromide (2.6 g, 11 mmol), and sodium nitirite (0.75 g, 11 mmol) were added to a solution of linoleic acid (3 g, 11 mmol, Nu-Chek Prep, Inc., Elysan, MN) in tetrahydrofuran:acetonitrile (1:1, 70 mL) at room temperature under nitrogen. After stirring for 4 h, the mixture was filtered and the solvent removed under vacuum. The resulting residue was dissolved in tetrahydrofuran (70 mL), and hydrogen peroxide (12.6 mL of a 30% solution, 110 mmol) was added with continuous stirring at 0 °C (ice bath). After 20 min, the solution was allowed to warm to room temperature; this crude mixture was extracted with hexane (2 × 200 mL), and the combined organic extracts were washed with saturated sodium chloride. The solvent was evaporated under vacuum and the crude product suspended in hexane:ether:acetic acid (70:30:1, v:v:v). The products were purified by silica gel (70−230 mesh) column chromatography using hexane:ether:acetic acid (70:30:1, v:v:v) as the solvent system. Fractions were analyzed on silica gel 60 plates (70−230 mesh; EM Science, Gibbstown NJ) developed twice in hexane:ether:acetic acid (70:30:1, v:v:v). Lipid products were visualized by UV_{254} and by 0.6% potassium dichromate in 55% sulfuric acid spray with charring. Fractions containing pure LNO_2 (R_f ~0.5) were combined, concentrated to give 1 g of LNO_2 (30% yield), and stored at −20 °C.

^{1}H NMR spectra were recorded on a Bruker DRX-500 spectrometer using a BBO or TBI probe equipped with *z* axis gradients and processed with XWINNMR 3.6. All acquisitions were carried out at 25 ± 1 °C. All spectra were referenced to the residual solvent peak of d-chloroform (^{1}H 7.26 ppm and ^{13}C 77.00 ppm). 1D ^{1}H and ^{13}C experiments were collected using standard Bruker parameter sets. The gradient selected 2D COSY, HMQC, and HMBC experiments were collected with 512 points in F1 and 2048 in F2. The 2D data were processed to 1024 × 1024 points using standard apodization functions in both dimensions.

HPLC/ESI/MS/MS. For direct infusion, LNO_2 was resuspended in methanol to a final concentration of 5 μM. The sample was injected directly into a Micromass Quattro II mass spectrometer equipped with a z spray source and triple quadrupole analyzer. The instrument was operated in the negative ionization mode with the capillary voltage set to 3.87 kV, the sampling cone set to 19 V, and the desolvation temperature set to 200 °C. For daughter ion analysis, the collision energy was 19 eV. For analysis of the GSH conjugate of LNO_2 (LNO_2−SG), HPLC/ESI/MS was utilized. HPLC was with a Hewlett-Packard 1100 equipped with a Discovery BIO Wide Pore C_{18} 3 μM, 15 cm × 2.1 mm (Supelco, Bellefonte, PA). The mobile phases consisted of 50% methanol, 50% water, 0.1% acetic acid (solvent A), and 100% methanol, 0.1% acetic acid (solvent B). Samples (25 μL) taken directly from the LNO_2 and GSH (see below) (Sigma-Aldrich, St. Louis, MO) reaction were chromatographed at 200 μL/min before entering the electrospray source. HPLC separation began at 100% solvent A (5 min), followed by a linear gradient to 100% solvent B (20 min), which was then held at 100% solvent B for 10 min. Approximately 12% of the HPLC eluate was diverted to the electrospray source operating in the positive ion mode and with the same parameters listed above. For daughter ion analysis of LNO_2−SG, the collision energy was 24 eV. HPLC/ESI/MS/MS analysis of LNO_2−SG was accomplished as above: for multiple reaction monitoring chromatograms, the precursor ion *m*/*z* 633 (LNO_2−SG) was selected and scanned for daughter ions at *m*/*z* 558, 504, and 457 as discussed in the text.

LNO_2−SG Formation: Synthesis and Kinetics. LNO_2 (40 μM) was reacted with 2 mM GSH in 0.1 M sodium phosphate buffer (pH = 7.5) for 1 min at 25 °C. For structural analysis, a 25 μL sample of the reaction was injected for HPLC/ESI/MS/MS as described above. For analytical and preparative HPLC, reactions were separated using a C18 column (Beckman, Ultrasphere ODS, 5 μm, 4.6 × 250 mm): chromatography was done at 0.6 mL/min with 100% solvent A (50% methanol, 0.05% TFA) for 5 min followed by a linear gradient to 100% solvent B (100% methanol, 0.05% TFA) over 15 min and held at 100% solvent B thereafter. Elutions were monitored at 274 nm. These analyses verified that the 1 min reactions described above resulted in complete conversion of LNO_2 (eluting at 27 min) to LNO_2−SG (eluting at 22 min). For kinetic analysis, the absorbance was measured every second between 245 and 295 nm on a DU 7400 UV−visible spectrophotometer (Beckman Coulter, Fullerton, CA). Reaction progression was monitored as increasing absorbance at 245 nm with conjugate formation. To obtain the pseudo-first-order rate constant, k_1, data were fitted to the equation

$$A_t = A_\infty - (A_\infty - A_0)\epsilon^{-k_1 t}$$

where A_t, A_∞, and A_0 are absorbances at time (t) equals t, ∞, and 0, respectively. The second-order rate constant, k_2, was calculated from k_1.

Radiolabeled LNO_2−SG was purified by preparative HPLC (above) from reactions (1 min, 25 °C) in 0.1 M sodium phosphate (pH 7.5) containing 200 μM LNO_2 and 50 μM total GSH (including [glycine-2-^{3}H]-GSH; final specific activity ~2.5 μCi/nmol).

Cell Lines and Culture. Cell lines used were parental MCF7 cells (MCF7/WT, MRP1-poor) and the derivative, MCF7/MRP1-10: a cell line stably transduced with a MRP1 expression vector as described previously (*22*). Cells were grown in Dulbecco's modified Eagle medium (DMEM) supplemented with 10% fetal bovine serum (FBS) at 37 °C, 5% CO_2.

Formation of LNO_2−SG in Cells. Cells (2 × 10^6/100 mm dish) were treated with 3 μM LNO_2 for $^1/_2$ h in Hanks buffered saline solution (with Mg, Ca, and glucose; Invitrogen). At the end of this incubation, cells were immediately washed three times in Hank's solution and lysed in 1 mL of methanol/acetic acid (99.9/0.1). Insoluble debris was pelleted from the methanol extract by centrifugation (12000*g*, 5 min, 4 °C) and the supernatant stored on dry ice until analysis by mass spectrometry.

MRP1-Mediated Transport Studies. ATP-dependent uptake of ^{3}H-LNO_2−SG into inside-out membrane vesicles isolated from MCF7/WT (MRP1-poor) and MCF7/MRP1-10 (transduced, MRP1 expressing) cells was accomplished as described previously (*22*, *23*). Results reported as ATP-dependent uptake were calculated by subtracting transport

in the presence of nonhydrolyzable ATP analogue, AMP-PCP, from transport observed in the presence of ATP.

PPARγ-Dependent Transcription Activation Assays. Cells were plated at a density of $1.0-1.5 \times 10^5$ cells per well in six-well dishes and grown for 24 h at 37 °C, 5% CO_2. Cells were then transfected with 1 μg of PPREx3-TK-LUC (*9*) plasmid or 1 μg of CMV-LUC (*24*) plasmid with or without 0.2 μg of pcDNA3-PPARγ (*25*) (kindly supplied by Dr. V. Krishna K. Chatterjee, Department of Medicine, University of Cambridge). The PPREx3-TK-LUC plasmid includes three PPAR responsive elements (PPRE) inserted upstream of a thymidine kinase promoter controlling transcription of the firefly luciferase gene. The control CMV-LUC plasmid contains the cytomegalovirus (CMV) promoter driving transcription of the firefly luciferase gene. For some experiments, cells were cotransfected with pSVβgal as a control for potential variations in transfection efficiency. Cells were transfected using Superfect reagent (Qiagen, Valencia, CA). Twenty-four hours after transfection, the cells were treated with 3 μM LNO_2 or vehicle control in 3 mL of Optimem (Invitrogen) for 1 h, at which time medium was replaced with Optimem minus LNO_2. Transfected cells were harvested 24 h after the start of induction (with LNO_2 or vehicle). Luciferase activity was determined using the Promega Luciferase Assay kit (Promega, Madison, WI) and a Turner TD-20/20 luminometer. β-Galactosidase activity was determined spectrophotometrically using the β-galactosidase enzyme assay system (Promega).

RESULTS

Synthesis and Analysis of LNO_2. Utilizing a previously published method to nitrate oleic acid (*17*) and a newly developed silica gel-based column chromatographic method, we synthesized and purified 1 g of LNO_2 (synthetic yield ~30%). HPLC, UV−visible spectroscopy (extinction coefficient = 10 100 cm^{-1} M^{-1} at 306 nm in 2% 1 M NaOH in MeOH), ESI/MS/MS (*m*/*z* = 324, negative ion mode), and thin-layer chromatography analysis confirmed a highly purified preparation of LNO_2 (97%). Direct infusion of LNO_2 into the mass spectrometer operating in the negative ion mode revealed one major peak at *m*/*z* 324 (Figure 1A), and collision-induced dissociation resulted in daughter ions including one at *m*/*z* 277 indicative of the denitrated anion of LNO_2 [(M − HNO_2) − H] (Figure 1B).

In contrast to a previous report (*19*), NMR analysis revealed a mixture of four, rather than two, regioisomers of nitration. As shown by ^{13}C NMR and ^{13}C APT, four resonances were observed between 150 and 152 ppm (Figure 2) which—based upon predicted chemical shifts and studies with nitrated oleic acid (*19*)—correspond to the four alternative nitrated vinyl carbons, C9, C10, C12, and C13 (Figure 3). A quadrupling of alkene peaks is also seen in the 120 to 140 ppm region (Figure 2): these peaks were assigned to the un-nitrated vinyl carbons. The quadrupling effect was also seen for the carbonyl carbons at 179.8 ppm (not shown). These data provide strong evidence for the presensce of four regioisomers of LNO_2 which were named as follows: external (E) designates isomers where the nitro group is positioned on the external position of one of the double bonds (E9 or E13) (Figure 3A), and internal (I) designates isomers where the nitro group is positioned on the internal position of the double bonds (I10 or I12) (Figure 3B).

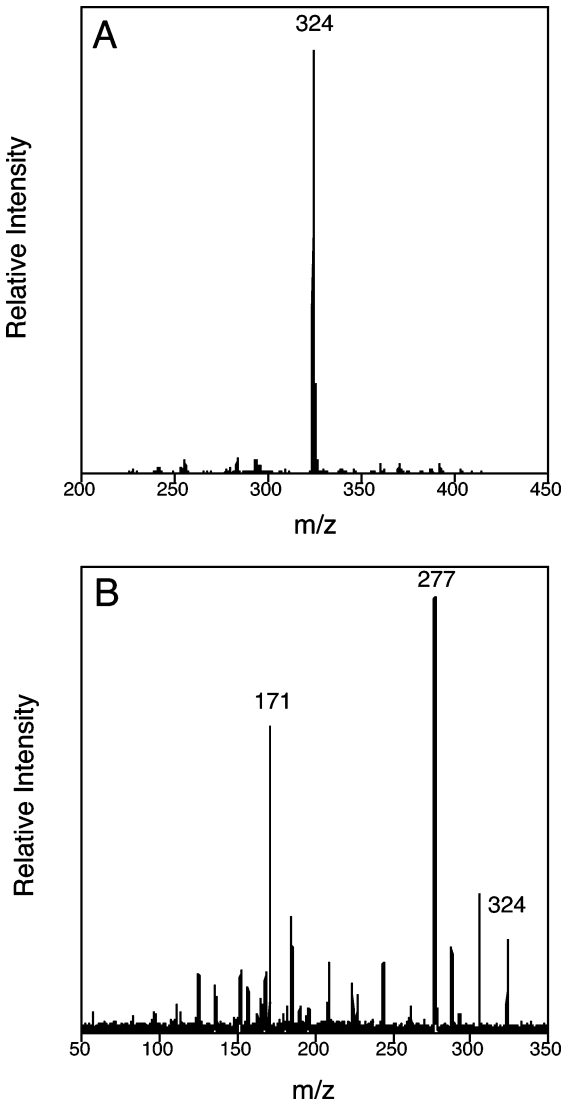

FIGURE 1: Mass spectrometry analysis of LNO_2. A 125 pmol sample of LNO_2 was injected directly into the MS operating in negative ion mode. Panel A shows the parent peak at 324 *m*/*z* [M − H] and panel B the daughter ions of the parent peak including 277 *m*/*z* [(M − HNO_2) − H].

1D and 2D COSY NMR enabled unambiguous assignment of protons to allylic and vinyl positions (C8−C14, Figure 3) as summarized in Table 1. The most downfield peaks were assigned to the vinyl protons β to the nitro group: the resonances at 7.08 and 7.02 corresponded to I and E type LNO_2, respectively. Due to overlap of the ^1H NMR spectra, these β vinyl protons were grouped together as I (9+13) and E (10+12). From 1D ^1H NMR, integration of these peaks revealed a 50:50 proportion of the I (9+13) and E (10+12) isomer groups. These data, together with ^{13}C spectra showing similar peak heights of the four isomers (Figure 2), strongly suggest that the four regioisomers are present in ~equal abundance.

Formation and Analysis of LNO_2−SG. After confirming the structure of LNO_2, we tested its ability to form conjugates with GSH under physiologically relevant conditions. Indeed, 40 μM LNO_2 reacted rapidly with 2 mM GSH in sodium phosphate buffer (pH = 7.5, 25 °C) as measured by absorbance changes between 245 and 295 nm. Analytical HPLC and HPLC/ESI/MS revealed quantitative conversion of the peak corresponding to LNO_2 to a more rapidly eluting

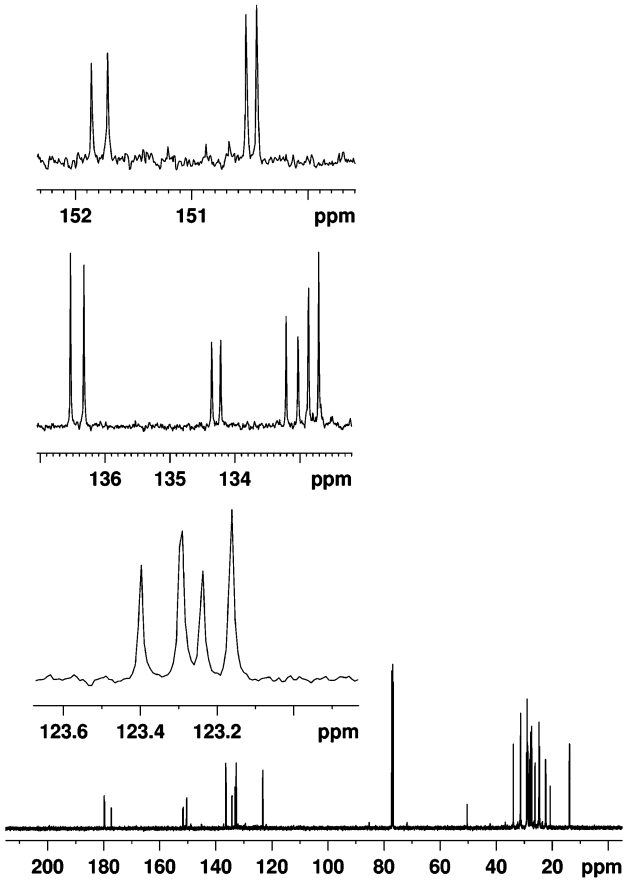

FIGURE 2: ^{13}C NMR analysis of LNO_2. Shown are the complete ^{13}C spectrum (lowest panel) and expanded regions showing four separate resonances in the nitro olefin region indicating the presence of four regioisomers of nitration. Resonances at 150−152 ppm correspond to nitrated vinyl carbons (uppermost panel) and at 120−140 ppm correspond to un-nitrated vinyl carbons (middle two panels).

peak corresponding to its glutathione conjugate, LNO_2−SG (633 *m*/*z*, positive ion mode) (Figure 4A). The kinetics of conjugation were monitored as absorbance changes at 245 nm, and from these data a pseudo-first-order rate constant of 0.38 s^{-1} was determined (Figure 5). From this a second-order rate constant of 190 s^{-1} M^{-1} was calculated.

MRP1 Mediates Efficient ATP-Dependent Transport of LNO_2−SG. Using inside-out plasma membrane vesicles, experiments shown in Figure 6 demonstrated that vesicles derived from MRP1-expressing, but not MRP-poor, cells could support ATP-dependent transport of LNO_2−SG (Figure 6A). Initial velocity analyses (Figure 6B) indicated that this transport was quite efficient: indeed, experiments yielded K_M (0.75 μM) and V_{max} (117 pmol·min^{-1}·mg^{-1} vesicle protein) values that compare favorably with those of other good MRP1 substrates obtained using similar vesicle preparations, substrates that include 15-d-PGJ_2−SG (K_M 1.4 μM, V_{max} 67 pmol·min^{-1}·mg^{-1}) (*21*) and leukotriene C4 (K_M ∼0.1 μM) (*26*, *27*).

Formation of LNO_2−SG in Cells. Tandem mass spectrometry was used to evaluate LNO_2−SG formation in intact cells. First, LNO_2−SG standards were synthesized in vitro and from these standards collision-induced dissociation spectra were obtained. As shown in Figure 4B, several prominent daughter ions resulted: they included *m*/*z* 558, 504, and 457 corresponding to fragments derived from

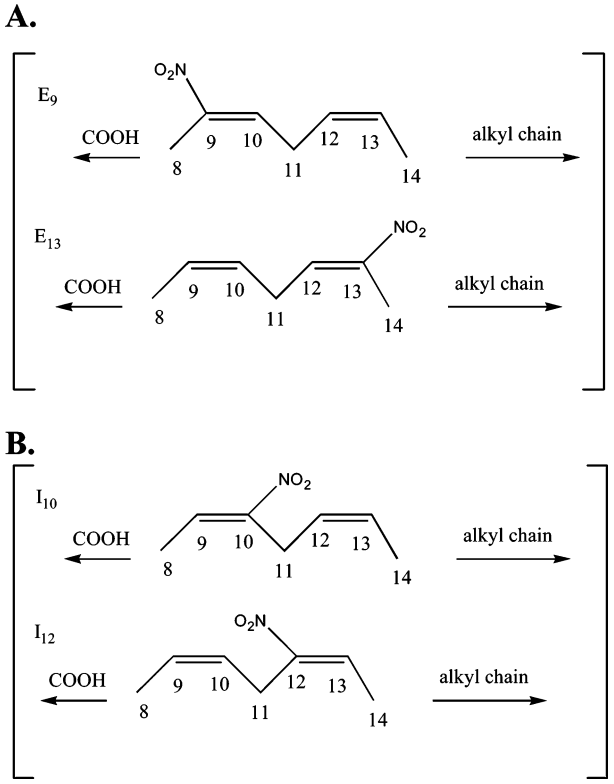

FIGURE 3: Structures of the four regioisomers of LNO_2. Shown are structures and carbon numbering for the four alternative isomers of LNO_2 in which the sites of nitration are on the external (E9 and E13, panel A) or internal (I10 or I12, panel B) portion of the double bond system.

Table 1: ^1H and ^{13}C NMR of LNO_2: Assignment of Resonance Peaks to Allylic and Vinyl Positions of the Four Positional Isomers of LNO_2[a]

carbon	^1H NMR (ppm)	^{13}C NMR (ppm)
E10,12	7.02	134.22, 134.36
E9,10[b] and E12,13[c]	5.49, 5.25	132.54−133.31, 123.06−123.47
E11	2.95	26.03
E8,14	2.59, 2.06	26.23
E9,13		151.72, 151.86
I9,13	7.08	136.32, 136.53
I9,10[d] and I12,13[e]	5.54, 5.32	132.54−133.31, 123.06−123.47
I11	3.33	24.73
I8,14	2.12	27.20−28.30
I10,12		150.44,150.53

[a] Resonance peaks were assigned using ^1H (1D, COSY, HMQC, and HMBC) and ^{13}C NMR. Alternative regioisomers are designated by the site of nitration as external (E9 or E13) or internal (I10 or I12) as defined in Figure 3. [b] C9 and C10 vinyl positions of E13 isomer. [c] C12 and C13 vinyl positions of E9 isomer. [d] C9 and C10 vinyl positions of I12 isomer. [e] C12 and C13 vinyl positions of I10 isomer.

scissions at positions 1, 2, and 2+3 illustrated in Figure 7A. These ions were used in the HPLC/ESI/MS/MS analysis to follow. MCF7 cells were treated with 3 μM LNO_2 for $^1/_2$ h. The cells were immediately washed in medium and intracellular LNO_2−SG extracted in methanol/acetic acid for HPLC/ESI/MS/MS. Multiple reaction monitoring chromatograms of material derived from MCF7/WT cells clearly demonstrated that LNO_2−SG is formed in cells (Figure 7B). Moreover, similarly treated MCF7/MRP1-10 cells also formed LNO_2−SG; however, integration of the ion current intensity chromatogram peaks showed that the levels of

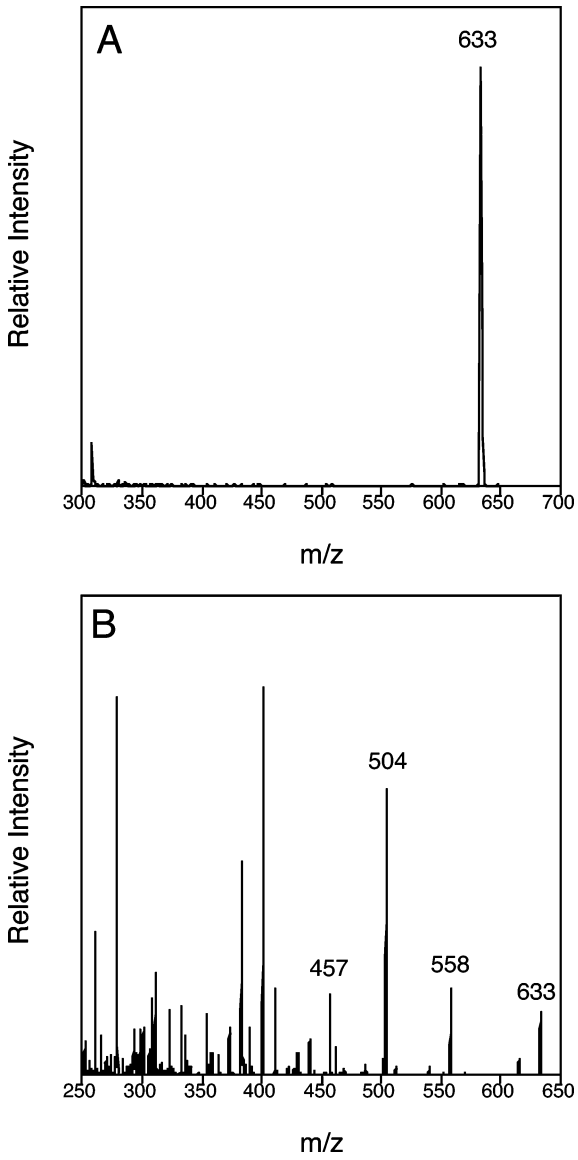

FIGURE 4: Mass spectrometry analysis of the LNO_2−SG. A 40 μM sample of LNO_2 was reacted with 2 mM glutathione in 0.1 M sodium phosphate buffer pH = 7.5 for 1 min at 25 °C. A 25 μL sample was analyzed by HPLC/ESI/MS as described in Experimental Procedures using the positive ion mode. Shown is the peak corresponding to the glutathione conjugate, LNO_2−SG (*m*/*z* 633, [M + H]) (panel A). Daughter ions of *m*/*z* 633 generated by collision-induced dissociation are shown in panel B.

intracellular LNO_2−SG accumulated by the end of the $^1/_2$ h LNO_2 treatment were considerably lower in MCF7/MRP1-10 cells than in MCF7/WT cells (MCF7/MRP1-10 levels were 15% of MCF7/WT levels, not shown). These data indicate that MRP1 is able to support active efflux of LNO_2−SG from intact cells.

Expression of MRP1 Inhibits LNO_2-Induced Activation of PPARγ-Dependent Transcription. Having established that LNO_2 is readily converted to its conjugate, LNO_2−SG, in the presence of physiologic concentrations of GSH, we next investigated whether expression of MRP1 would influence—at the cellular level—LNO_2-induced activation of PPARγ-dependent transcription. First, using MRP1-poor MCF7/WT cells, we verified that LNO_2 selectively induced the expression of a transiently transfected PPAR-responsive (PPRE-containing; PPREx3-TK-LUC), but not a control (CMV-LUC), reporter gene (Figure 8A). These data, showing ~87-fold induction of the PPAR-responsive reporter gene by 3 μM LNO_2, indicate that LNO_2 is a much more potent PPARγ activator than is 15-d-PGJ_2, a PPARγ ligand that at 20 μM in similar experiments resulted in ~16-fold induction (*21*). To further investigate the contribution of PPARγ to LNO_2-induced gene activation, we cotransfected the PPRE-containing reporter gene with a PPARγ expression vector. Inclusion of PPARγ greatly augmented induction (6.2-fold), indicating that LNO_2-induced gene activation is indeed mediated by PPARγ (Figure 8A). Last, to assess the effect of MRP1, MCF7/WT and MCF7/MRP1-10 cells were cotransfected with PPARγ and the PPRE-containing reporter gene followed by treatment with LNO_2 or vehicle. As shown in Figure 8B, expression of MRP1 (MCF7/MRP1-10 cells) greatly inhibited LNO_2-induced PPARγ-dependent transcription. These data indicate that GSH conjugation of LNO_2 and the subsequent efflux of this conjugate by MRP1 can profoundly attenuate the transcriptional activating effects of this signaling lipid molecule.

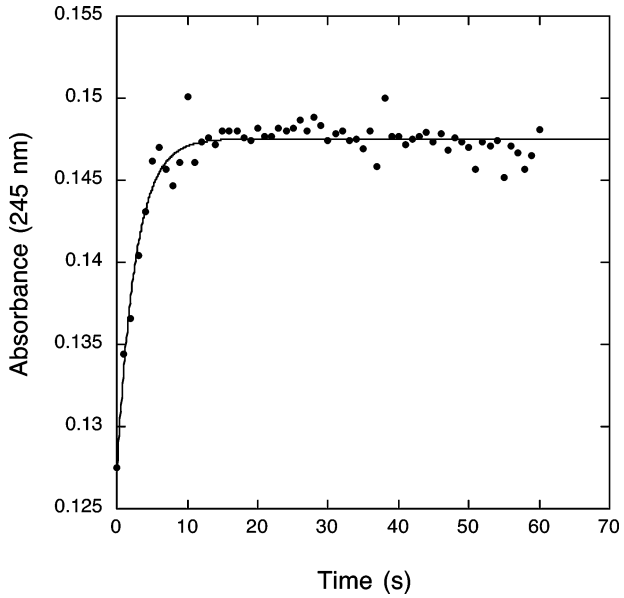

FIGURE 5: Kinetics of LNO_2−SG formation. LNO_2 (40 μM) was reacted with 2 mM glutathione in sodium phosphate buffer (pH = 7.5) at 25 °C. Reaction progress was monitored by the change in absorbance at 245 nm and the data fitted to pseudo-first-order kinetics as described in Experimental Procedures.

DISCUSSION

Recent reports have suggested that nitrated unsaturated lipids such as LNO_2 and OA-NO_2 have antiinflammatory, antiplatelet, and vasodilation activities (*13*−*16*). In addition, these lipids can regulate the expression of specific endogenous as well as PPAR-dependent reporter genes (*17*, *18*, *28*). The mechanisms by which these activities are mediated are attributed to various alternative or overlapping signaling pathways including cyclic nucleotide-dependent pathways, nitric oxide release, and direct interaction with cellular receptors such as PPAR and perhaps others (*14*, *18*, *28*, *29*). Enthusiasm for the physiological relevance of these compounds is greatly enhanced by the observations that LNO_2 and OA-NO_2 are formed and can accumulate to relatively high levels (high nano- to low micromolar) in blood and plasma (*17*, *19*).

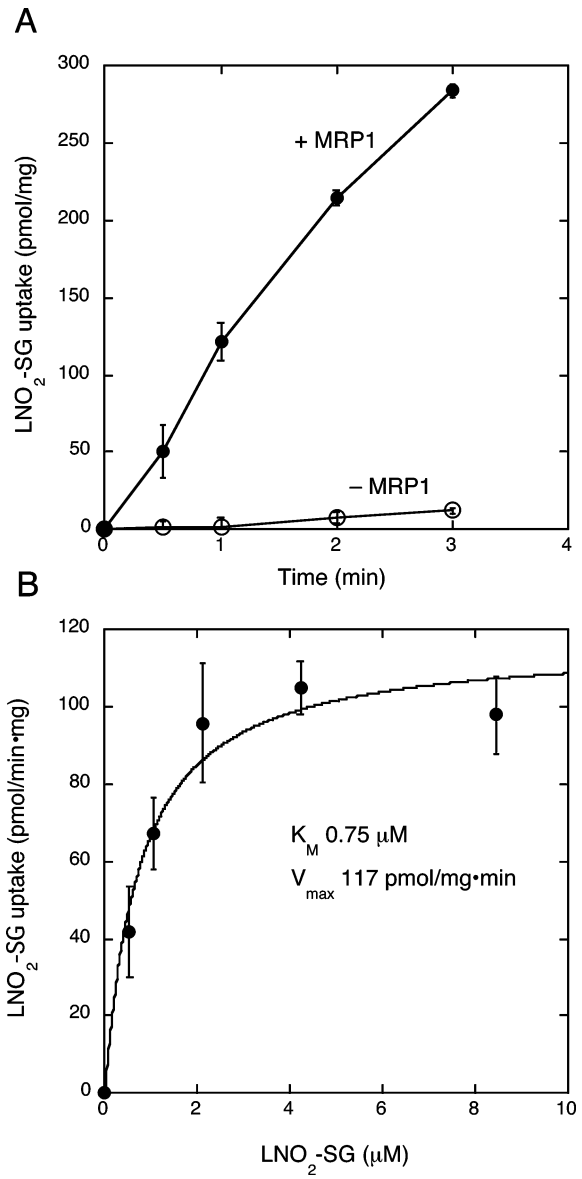

FIGURE 6: ATP-dependent, MRP1-mediated transport of LNO_2−SG. ATP-dependent transport of ^{3}H-labeled LNO_2−SG was accomplished using inside-out plasma membrane vesicles as described in Experimental Procedures. Panel A shows the time course of ATP-dependent LNO_2−SG (2.3 μM) transport using vesicles derived from MRP-poor (−MRP1, open circles) MCF7/WT and MRP1-expressing (+MRP1, closed circles) MCF7/MRP1-10 cells. Panel B shows the initial velocities of ATP-dependent, MRP1-mediated (vesicles from MCF7/MRP1-10 cells) LNO_2−SG transport as a function of LNO_2−SG concentration. Data are represented as the mean values ± 1 SD of at least 3 independent determinations.

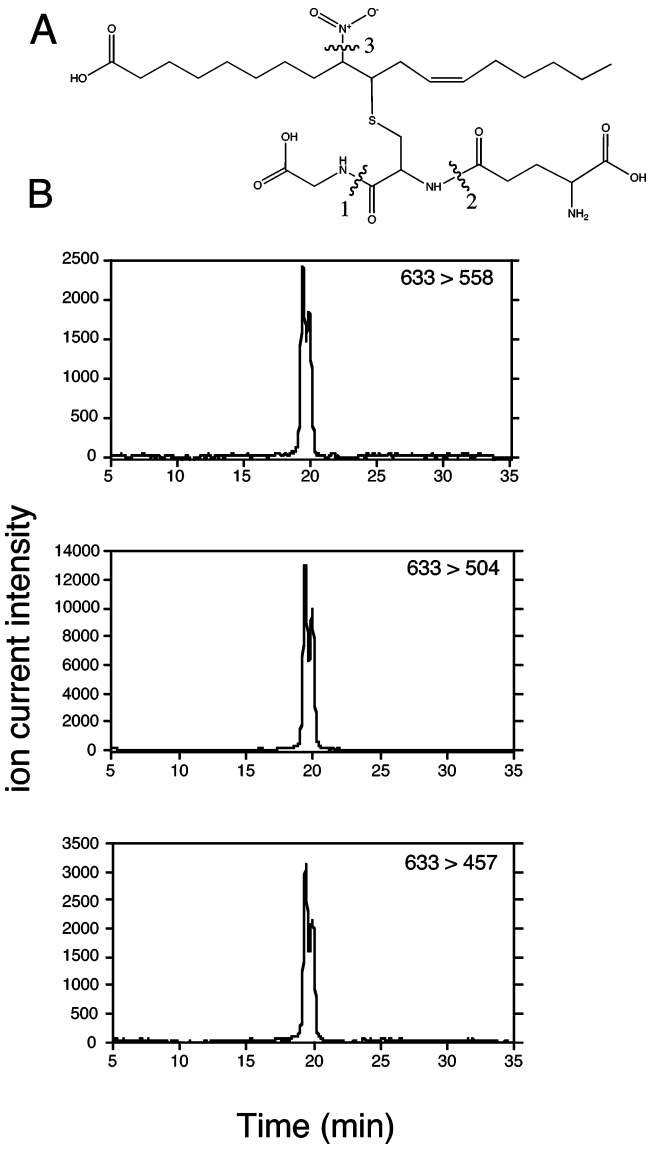

FIGURE 7: LNO_2−SG formation in MCF7/WT cells. MCF7/WT cells were treated with 3 μM LNO_2 for $^1/_2$ h followed by lysis and extraction of intracellular material in methanol/acetic acid (99.9/0.1, v/v). LNO_2−SG was detected from these extracts using HPLC/ESI/MS/MS as described in Experimental Procedures. (A) Shown are the structure of LNO_2−SG and the positions of fragmentation yielding the prominent daughter ions used for multiple reaction monitoring: these daughter ions of *m*/*z* 633 (LNO_2−SG) include *m*/*z* 558 (fragmentation at 1, loss of glycyl group), *m*/*z* 504 (fragmentation at 2, loss of glutamyl group), and *m*/*z* 457 (fragmentations at 2+3, loss of glutamyl and nitrate groups). (B) Shown are multiple reaction monitoring HPLC/ESI/MS/MS chromatograms of intracellular extracts derived from LNO_2-treated MCF7/WT cells. Ion current intensities are expressed as arbitrary units on the ordinate. The precursor ion, *m*/*z* 633, corresponding to LNO_2−SG was selected for all chromatograms and scanned for the daughter ions (*m*/*z* 558, 504, and 457) described above. The elution times for the chromatogram peaks so defined were identical to those obtained using a LNO_2−SG standard synthesized in vitro (not shown).

In the present study we have used PPARγ-dependent transcription activation as a measure of LNO_2 bioactivity. LNO_2 is a particularly attractive potential ligand to study as it is among the most potent endogenous lipid activators of PPARγ yet described (*18*). Moreover, the reported levels of LNO_2 formed in vivo are sufficient to effect this PPAR-dependent transactivation. Herein we find that this electrophilic lipid readily reacts—under physiological conditions, in vitro and in cells—with GSH to form LNO_2−SG. As intracellular levels of GSH are quite high (1−10 mM), most of the available intracellular LNO_2 is expected to be bound as adducts with GSH or other cellular nucleophiles (e.g. protein thiols). However, formation of these LNO_2−SG adducts is insufficient to block PPARγ-dependent transcription activation as evidenced by the present studies using MCF7/WT cells, as well as previous work (*18*), which show strong induction of a PPRE-containing reporter gene by LNO_2. Expression of MRP1—a plasma membrane-associated transport protein which supports efficient efflux of LNO_2−SG—results in profound attenuation of LNO_2-induced PPARγ-

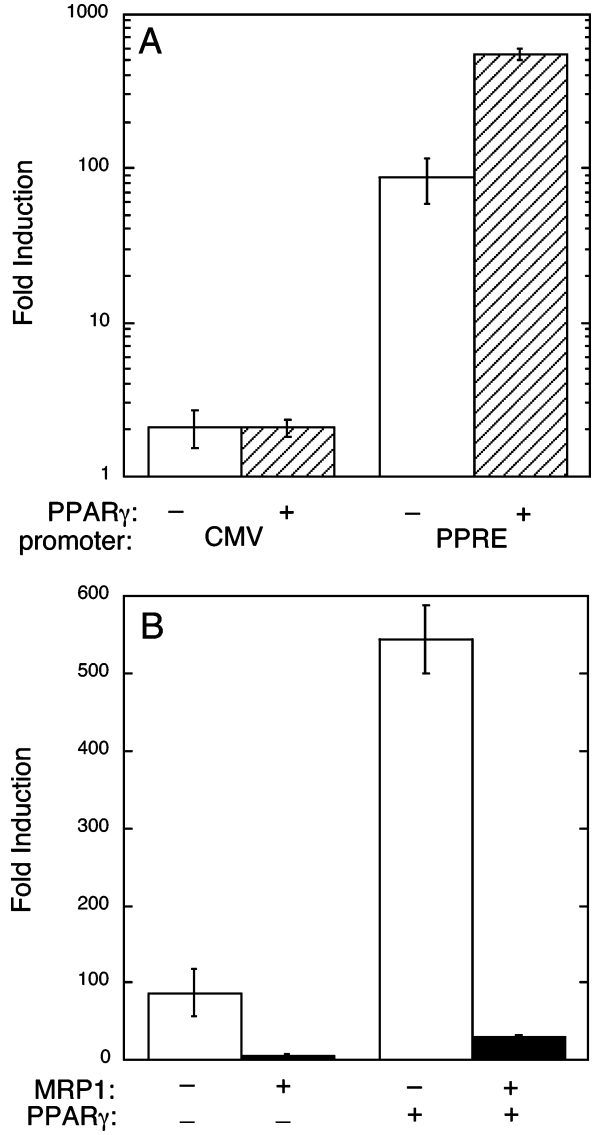

FIGURE 8: MRP1 expression inhibits LNO_2-induced, PPARγ-dependent transcription activation. MCF7 cells were transfected with 1 μg of luciferase reporter gene driven by either the CMV (control) or PPAR-responsive (PPRE-containing) promoters. Reporters were cotransfected with either PPARγ expression or empty vectors (0.2 μg) as indicated. Twenty-four hours later, cells were treated with 3 μM LNO_2 or vehicle for 1 h: cells were harvested for luciferase assay 24 h after this treatment. Luciferase activities were normalized to protein concentration or, in some experiments, to β-galactosidase activity of cells cotransfected with pSVβgal. Data are reported as fold induction, a value defined as normalized luciferase activity in cells treated with LNO_2 divided by activity of cells treated with vehicle alone. Shown are data derived from representative experiments. Each bar represents the mean of 3 independent transfections ± 1 SD. (A) MRP1-poor MCF7/WT cells were transfected with CMV-LUC or PPRE-LUC plus (+, crosshatched bars) or minus (−, open bars) cotransfection with PPARγ as indicated. (B) MRP1-poor MCF7/WT (MRP1−, open bars) or MRP1-expressing MCF7/MRP1-10 (MRP1+, dark bars) cells were transfected with PPRE-LUC plus (+) or (−) cotransfection with PPARγ as indicated.

dependent transcription, suggesting that conjugate removal is the key limiting step for inhibition of LNO_2 activity. While our studies have focused on PPARγ-dependent transactivation, it is likely that GSH conjugation and MRP1-mediated efflux will also be important determinants of cellular responses to PPAR-independent activities of LNO_2 and other nitroalkene lipids.

In contrast to an earlier report (*19*), ^{1}H and ^{13}C NMR analysis revealed that the LNO_2 formed by chemical synthesis consists of four, rather than two, regioisomers of nitration: each of the four isomers is present in ~equal abundance. While nitration may also occur by an as yet unrecognized isomer-selective enzymatic process, our data indicate that in vivo chemical nitration will result in the formation of all four regioisomers of LNO_2. What is not known is whether or not the various regioisomers have equivalent bioactivities. While the ability to donate nitric oxide via spontaneous decomposition might be expected to be similar, it would not be surprising to find qualitative or quantitative differences in LNO_2−receptor interactions among the four regioisomers of LNO_2.

ACKNOWLEDGMENT

The authors are grateful to Bob Wykle for helpful discussions and to Mike Samuels and Mike Thomas for their help with the mass spectrometry.

REFERENCES

1. Chen, Y. E., Fu, M., Zhang, J., Zhu, X., Lin, Y., Akinbami, M. A., and Song, Q. (2003) Peroxisome proliferator-activated receptors and the cardiovascular system, *Vitam. Horm. 66*, 157−188.
2. Evans, R., Barish, G., and Wang, Y. (2004) PPARs and the complex journey to obesity. *Nat. Med. 10*, 355−361.
3. Kliewer, S. A., Lehmann, J., uuml, rgen, M., and Willson, T. M. (1999) Orphan Nuclear Receptors: Shifting Endocrinology into Reverse, *Science 284*, 757−760.
4. Fu, M. G., Zhang, J. F., Zhu, X. J., Myles, D. E., Willson, T. M., Liu, X. D., and Chen, Y. Q. E. (2001) Peroxisome proliferator-activated receptor gamma inhibits transforming growth factor β-induced connective tissue growth factor expression in human aortic smooth muscle cells by interfering with Smad3, *J. Biol. Chem. 276*, 45888−45894.
5. Chawla, A., Repa, J. J., Evans, R. M., and Mangelsdorf, D. J. (2001) Nuclear Receptors and Lipid Physiology: Opening the X-Files, *Science 294*, 1866−1870.
6. Kodera, Y., Takeyama, K.-i., Murayama, A., Suzawa, M., Masuhiro, Y., and Kato, S. (2000) Ligand type-specific Interactions of Peroxisome Proliferator-activated Receptor gamma with Transcriptional Coactivators, *J. Biol. Chem. 275*, 33201−33204.
7. Qi, C., Zhu, Y., and Reddy, J. K. (2000) Peroxisome proliferator-activated receptors, coactivators, and downstream targets, *Cell Biochem. Biophys. 32 Spring*, 187−204.
8. Lehmann, J. M., Moore, L. B., Smith-Oliver, T. A., Wilkison, W. O., Willson, T. M., and Kliewer, S. A. (1995) An Antidiabetic Thiazolidinedione Is a High Affinity Ligand for Peroxisome Proliferator-activated Receptor γ (PPARγ), *J. Biol. Chem. 270*, 12953−12956.
9. Forman, B. M., Tontonoz, P., Chen, J., Brun, R. P., Spiegelman, B. M., and Evans, R. M. (1995) 15-Deoxy-delta 12, 14-prostaglandin J2 is a ligand for the adipocyte determination factor PPAR gamma, *Cell 83*, 803−812.
10. Kliewer, S. A., Lenhard, J. M., Willson, T. M., Patel, I., Morris, D. C., and Lehmann, J. M. (1995) A prostaglandin J2 metabolite binds peroxisome proliferator-activated receptor gamma and promotes adipocyte differentiation, *Cell 83*, 813−819.
11. McIntyre, T. M., Pontsler, A. V., Silva, A. R., St. Hilaire, A., Xu, Y., Hinshaw, J. C., Zimmerman, G. A., Hama, K., Aoki, J., Arai, H., and Prestwich, G. D. (2003) From the Cover: Identification of an intracellular receptor for lysophosphatidic acid (LPA): LPA is a transcellular PPARgamma agonist, *Proc. Natl. Acad. Sci. U.S.A. 100*, 131−136.
12. Nagy, L., Tontonoz, P., Alvarez, J. G., Chen, H., and Evans, R. M. (1998) Oxidized LDL regulates macrophage gene expression through ligand activation of PPARgamma, *Cell 93*, 229−240.
13. Coles, B., Bloodsworth, A., Clark, S. R., Lewis, M. J., Cross, A. R., Freeman, B. A., and O'Donnell, V. B. (2002) Nitrolinoleate Inhibits Superoxide Generation, Degranulation, and Integrin Expression by Human Neutrophils: Novel Antiinflammatory

Properties of Nitric Oxide-Derived Reactive Species in Vascular Cells, *Circ. Res. 91*, 375−381.
14. Coles, B., Bloodsworth, A., Eiserich, J. P., Coffey, M. J., McLoughlin, R. M., Giddings, J. C., Lewis, M. J., Haslam, R. J., Freeman, B. A., and O'Donnell, V. B. (2002) Nitrolinoleate Inhibits Platelet Activation by Attenuating Calcium Mobilization and Inducing Phosphorylation of Vasodilator-stimulated Phosphoprotein through Elevation of cAMP, *J. Biol. Chem. 277*, 5832−5840.
15. Lim, D. G., Sweeney, S., Bloodsworth, A., White, C. R., Chumley, P. H., Krishna, N. R., Schopfer, F., O'Donnell, V. B., Eiserich, J. P., and Freeman, B. A. (2002) Nitrolinoleate, a nitric oxide-derived mediator of cell function: Synthesis, characterization, and vasomotor activity, *Proc. Natl. Acad. Sci. U.S.A. 99*, 15941−15946.
16. Lima, E. S., Bonini, M. G., Augusto, O., Barbeiro, H. V., Souza, H. P., and Abdalla, D. S. (2005) Nitrated lipids decompose to nitric oxide and lipid radicals and cause vasorelaxation, *Free Radical Biol. Med. 39*, 532−539.
17. Baker, P. R. S., Lin, Y., Schopfer, F. J., Woodcock, S. R., Groeger, A. L., Batthyany, C., Sweeney, S., Long, M. H., Iles, K. E., Baker, L. M. S., Branchaud, B. P., Chen, Y. E., and Freeman, B. A. (2005) Fatty Acid Transduction of Nitric Oxide Signaling: Multiple nitrated unsaturated fatty acid derivatives exist in human blood and urine and serve as endogenous peroxisome proliferator-activated receptor ligands, *J. Biol. Chem. 280*, 42464−42475.
18. Schopfer, F. J., Lin, Y., Baker, P. R. S., Cui, T., Garcia-Barrio, M., Zhang, J., Chen, K., Chen, Y. E., and Freeman, B. A. (2005) Nitrolinoleic acid: An endogenous peroxisome proliferator-activated receptor γ ligand, *Proc. Natl. Acad. Sci. U.S.A. 102*, 2340−2345.
19. Baker, P. R. S., Schopfer, F. J., Sweeney, S., and Freeman, B. A. (2004) Red cell membrane and plasma linoleic acid nitration products: Synthesis, clinical identification, and quantitation, *Proc. Natl. Acad. Sci. U.S.A. 101*, 11577−11582.
20. Paumi, C., Smitherman, P., Townsend, A., and Morrow, C. (2004) Glutathione S-transferases (GSTs) inhibit transcriptional activation by the peroxisomal proliferator-activated receptor gamma (PPAR gamma) ligand, 15-deoxy-Delta(12,14)prostaglandin J(2) (15-d-PGJ(2)), *Biochemistry 43*, 2345−2352.
21. Paumi, C. M., Wright, M., Townsend, A. J., and Morrow, C. S. (2003) Multidrug Resistance Protein (MRP) 1 and MRP3 Attenuate Cytotoxic and Transactivating Effects of the Cyclopentenone Prostaglandin, 15-Deoxy-Delta(12,14)Prostaglandin J(2) in MCF7 Breast Cancer Cells, *Biochemistry 42*, 5429−5437.
22. Smitherman, P. K., Townsend, A. J., Kute, T. E., and Morrow, C. S. (2004) Role of Multidrug Resistance Protein 2 (MRP2, ABCC2) in Alkylating Agent Detoxification: MRP2 Potentiates Glutathione S-Transferase A1-1-Mediated Resistance to Chlorambucil Cytotoxicity, *J. Pharmacol. Exp. Ther. 308*, 260−267.
23. Paumi, C. M., Ledford, B. G., Smitherman, P. K., Townsend, A. J., and Morrow, C. S. (2001) Role of Multidrug Resistance Protein 1 (MRP1) and Glutathione S-Transferase A1−1 in Alkylating Agent Resistance. Kinetics of glutathione conjugate formation and efflux govern differential cellular sensitivity to chlorambucil versus melphalan toxicity, *J. Biol. Chem. 276*, 7952−7956.
24. Liu, J. M., Fujii, H., Green, S. W., Komatsu, N., Young, N., and Shimada, T. (1991) Indiscriminate activity from the B19 parvovirus P6 promoter in nonpermissive cells, *Virology 182*, 361−364.
25. Gurnell, M., Wentworth, J. M., Agostini, M., Adams, M., Collingwood, T. N., Provenzano, C., Browne, P. O., Rajanayagam, O., Burris, T. P., Schwabe, J. W., Lazar, M. A., and Chatterjee, V. K. K. (2000) A Dominant-negative Peroxisome Proliferator-activated Receptor gamma (PPARgamma) Mutant Is a Constitutive Repressor and Inhibits PPARgamma -mediated Adipogenesis, *J. Biol. Chem. 275*, 5754−5759.
26. Leier, I., Jedlitschky, G., Buchholz, U., Cole, S. P., Deeley, R. G., and Keppler, D. (1994) The MRP gene encodes an ATP-dependent export pump for leukotriene C4 and structurally related conjugates, *J. Biol. Chem. 269*, 27807−27810.
27. Loe, D. W., Almquist, K. C., Deeley, R. G., and Cole, S. P. C. (1996) Multidrug resistance protein (MRP)-mediated transport of leukotriene C4 and chemotherapeutic agents in membrane vesicles: demonstration of glutathione-dependent vincristine transport, *J. Biol. Chem. 271*, 9675−9682.
28. Wright, M. M., Schopfer, F. J., Baker, P. R. S., Vidyasagar, V., Powell, P., Chumley, P., Iles, K. E., Freeman, B. A., and Agarwal, A. (2006) Fatty acid transduction of nitric oxide signaling: Nitrolinoleic acid potently activates endothelial heme oxygenase 1 expression, *Proc. Natl. Acad. Sci. U.S.A. 103*, 4299−4304.
29. O'Donnell, V. B., and Freeman, B. A. (2001) Interactions Between Nitric Oxide and Lipid Oxidation Pathways: Implications for Vascular Disease, *Circ. Res. 88*, 12−21.

BI0605639